Check for updates

Energy Storage

WILEY

ENERGY STORAGE

REVIEW

Potential of the Use of Sodium Chloride (NaCl) in Thermal Energy Storage Applications

Luisa F. Cabeza[1] | Franklin R. Martínez[1,2] | Gabriel Zsembinszki[1] | Emiliano Borri[1]

[1]GREiA Research Group, Universitat de Lleida, Lleida, Spain | [2]Center for Advanced Study of Lithium and Industrial Minerals (CELiMIN), University of Antofagasta, Antofagasta, Chile

Correspondence: Luisa F. Cabeza (luisaf.cabeza@udl.cat)

Received: 28 August 2024 | **Revised:** 16 October 2024 | **Accepted:** 27 October 2024

Funding: This work was supported by the Ministerio de Ciencia e Innovación—Agencia Estatal de Investigación (AEI) (PID2021-123511OB-C31—MCIN/AEI/10.13039/501100011033/FEDER, UE), and Ministerio de Ciencia e Innovación—Agencia Estatal de Investigación (AEI) (RED2022-134219-T).

Keywords: applications | latent TES | sensible TES | sodium chloride | thermal energy storage

ABSTRACT

Energy storage is a group of technologies that decrease the gap between energy supply and energy demand. Thermal energy storage (TES) reduces this gap at not only different temperatures but also at different places or power. Design criteria include the integration of the storage system into the whole application system, maximum load, and high-energy density. Since energy density is given by the material used, the selection of the storage material is key to the success of any energy storage system. In this paper, the potential of sodium chloride (NaCl) to be used in TES, both using sensible TES and latent TES, is evaluated for low-temperature applications and for high-temperature ones. This material is found to have high potential for successful *applications*, both in buildings and in industry.

1 | Introduction

Energy storage technologies have the objective of harvesting energy, storing it between a few hours up to several weeks, and releasing it to be used again [1]. The main goal of energy storage is to reduce the gap in time between energy supply and demand, but it can also be used to decrease the gap in location or in power. Moreover, since energy storage helps in reducing energy consumption and increasing the energy efficiency of systems, these technologies are very important tools in the decarbonization of our planet. Energy storage, on the other hand, can be included in all steps of the energy system, it can contribute to the production step, to the electricity grid, to heating and cooling networks, and to increase the efficiency of demand-side management tools. Energy storage technologies include electrical and electromagnetic energy storage, electrochemical energy storage, hydrogen energy storage, mechanical energy storage, and thermal energy storage (TES). Finally, energy storage is implemented in power applications (where high-power output is needed for a relatively short period of time) or in energy applications (that require much longer discharge times).

TES systems store thermal energy (heat or cold) to be used at a later time, at a different temperature, in a different place, or with different power [2]. It is important to highlight that as in any energy storage system, a complete TES storage cycle involves three steps: charge, storage, and discharge. Even though the three steps are essential in any application, charging and discharging are mainly related to the power in the system, and storage is mainly related to the energy density of the system.

The design of a TES system asks for several requirements such as high-energy density in the storage material (also known as storage capacity), mechanical and chemical stability of the storage material, complete cycle reversibility, good heat transfer between the HTF and the storage material, compatibility between the storage the container material, low thermal losses, and easy control [2]. Design criteria to also be considered include the

© 2024 John Wiley & Sons Ltd.

TABLE 1 | Typical materials used in sensible TES (adapted from [10]).

Material salt composition in wt.%	Melting temperature [°C]	Heat capacity [kJ/kg K]	Stability limit [°C]
60 wt.% NaNO3+40 wt.% KNO3	223	1.5 (@400°C)	565
32 wt.% K_2CO_3+35 wt.% Li_2CO_3+33 wt.% Na_2CO_3	397	1.9 (@700°C)	> 650
59 wt.% KF+29 wt.% LiF+12 wt.% NaF	454	1.9 (@700°C)	> 700
23.9 wt.% KCl+7.5 wt.% NaCl+68.6 wt.% $ZnCl_2$	204	0.8 (@300°C–600°C)	850
20.4 wt.% KCl+55.1 wt.% $MgCl_2$+24.5 wt.% NaCl	380	1.0 (@500°C–800°C)	800

TABLE 2 | Proposed materials used in sensible TES for CSP plants.

Material	Melting temperature [°C]	Heat capacity [kJ/kg·K]	Stability limit [°C]	Reference
23.9 wt.% KCl+7.5 wt.% NaCl +68.6 wt.% ZnCl2	204	0.8 (@300°C–600°C)	850	[10, 11]
20.4 wt.% KCl+55.1 wt.% $MgCl_2$+24.5 wt.% NaCl	380	1.0 (@500°C–800°C)	800	[10]
17.8 wt.% KCl+68.2 wt.% $MgCl_2$+14.0 wt.% NaCl	380	n.a.	> 800	[12, 13]
7.5 wt.% NaCl+23.9 wt.% KCl+68.6 wt.% $ZnCl_2$	477	0.81	n.a.	[14]
5.57 wt.% LiCl+13.14 wt.% NaCl +81.29 wt.% $ZnCl_2$	495	1.06	n.a.	[14]
39.05wt.%NaCl+14.94 wt.% $CaCl_2$+46.01 wt.% $ZnCl_2$	645	0.94	n.a.	[14]

Abbreviation: n.a. – not available.

nominal temperature and enthalpy change, the operation strategy, the integration into the application system, and the maximum load needed.

When implementing storage in an energy system several benefits can be obtained, such as better efficiency by achieving a more efficient use of energy; better economics by reducing capital and operational costs; better system performance and reliability; and less pollution of the environment and less CO_2 emissions, contributing to the mitigation of climate change.

Literature lists different key performance indicators (KPIs) to be used to evaluate TES systems [3, 4]. The first one is the specific energy or the energy stored per unit mass of the system; mobile systems (e.g., vehicles and aircraft) require high specific energy, while for stationary systems (i.e., grid-level and utility-level systems) this is insignificant. Energy density, or the energy stored per unit of volume, measures how big the storage system needs to be; it is important for mobile applications as well as for distributed storage. Round-trip efficiency

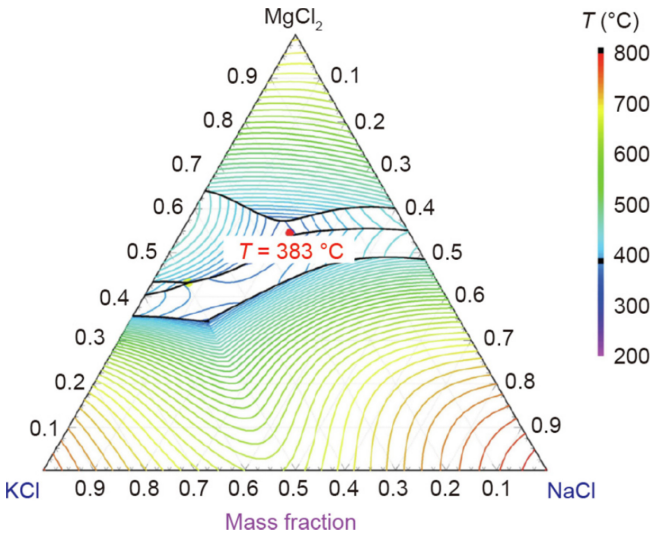


FIGURE 1 | Phase diagram of $MgCl_2$/KCl/NaCl modeled with FactSage [15].

25784862, 2024, 8, Downloaded from https://onlinelibrary.wiley.com/doi/10.1002/est2.70091 by Makerere University, Wiley Online Library on [01/11/2026]. See the Terms and Conditions (https://onlinelibrary.wiley.com/terms-and-conditions) on Wiley Online Library for rules of use; OA articles are governed by the applicable Creative Commons License

(or efficiency) is the ratio of the energy output of the storage system to the energy input and it can be expressed as the product of the charging efficiency and the generating efficiency. Another interesting KPI is the maximum depth of discharge, that is, the fraction of energy stored that can be reused; useful discharge capacity seems to be around 80% of the rated capacity since manufacturers tend to recommend avoiding full discharge of systems such as batteries. The cycle life indicates how many times the storage system may be charged and discharged before its round-trip efficiency and its storage capacity deteriorate. Finally, the self-discharge time is the time for a fully charged system to discharge to a defined depth of discharge, when it does not supply any useful energy; it can vary from 20% in flywheels to infinite in pump-hydro storage systems.

Recently the need for TES systems for high-temperature systems has raised importance for practitioners, pushing researchers to find materials for high-temperature TES [5, 6], and between the several options found in the literature, NaCl withstands due to its characteristics and properties such as being an inorganic material with low cost and high availability [7]. This paper aims to assess all literature concerning NaCl use as TES material to help researchers and practitioners use it in the right way or to further develop and study this material in TES.

2 | NaCl in TES

Literature suggests that NaCl may be used in TES as sensible heat and latent heat storage.

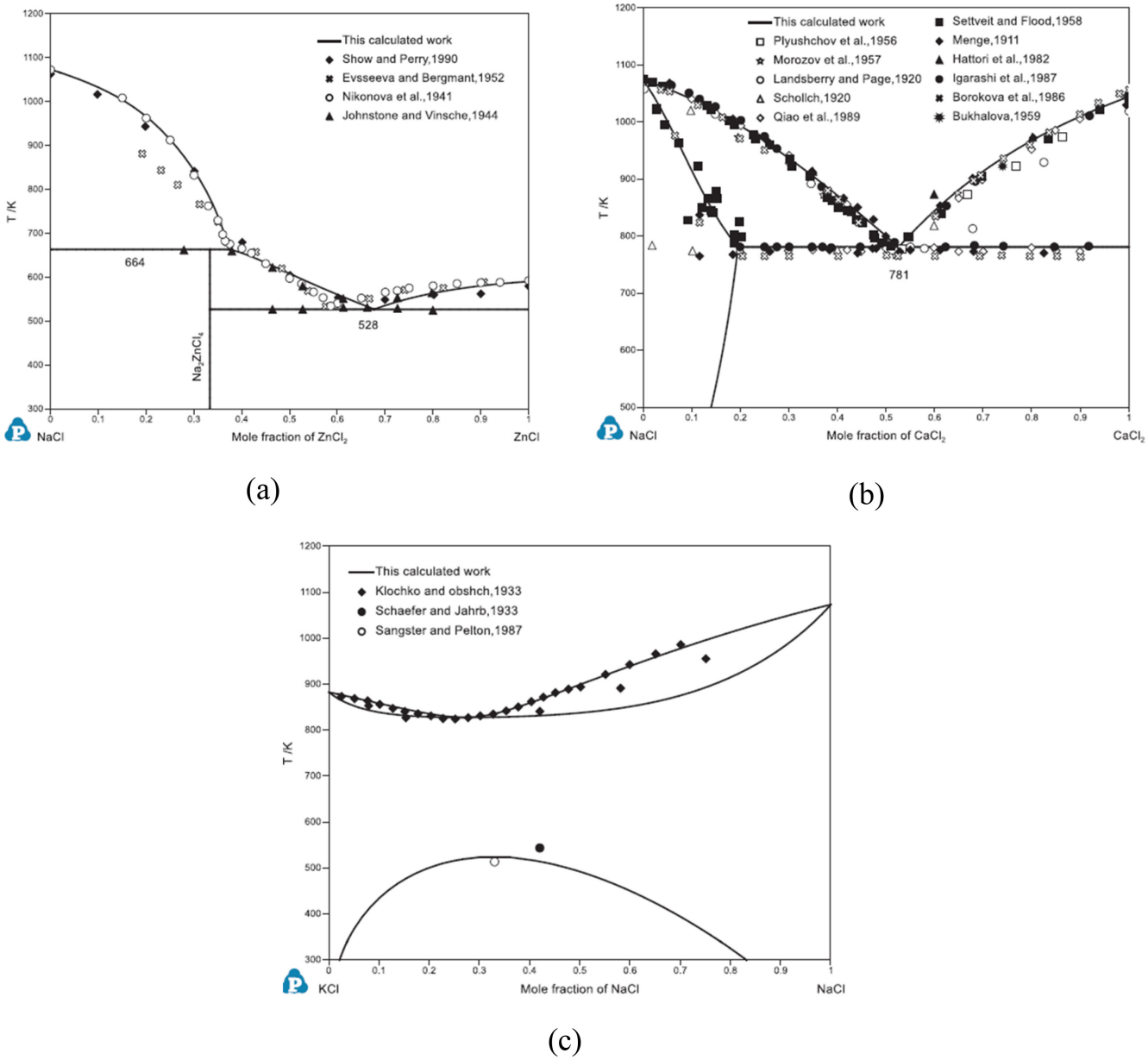


FIGURE 2 | (a) NaCl–$ZnCl_2$ phase diagram; (b) NaCl–$CaCl_2$ phase diagram; and (c) LiCl–NaCl phase diagram [14].

25784862, 2024, 8, Downloaded from https://onlinelibrary.wiley.com/doi/10.1002/est2.70091 by Makerere University, Wiley Online Library on [01/11/2026]. See the Terms and Conditions (https://onlinelibrary.wiley.com/terms-and-conditions) on Wiley Online Library for rules of use; OA articles are governed by the applicable Creative Commons License

2.1 | NaCl In Sensible TES Applications

One of the most mature TES applications is the use of molten salts in concentrating solar power (CSP) plants. Such materials have requirements such as high thermal stability, a large range of temperatures in the liquid state, low viscosity, low vapor pressure, high heat capacity, low corrosion rates, the ability to form homogeneous mixtures by dissolving a large amount of compounds, both organic and inorganic, and low production costs [8].

Picard [9] carried out one of the first studies on molten salt mixtures. He studied the mixture 53 wt.% KNO_3+40 wt.% $NaNO_2$+7 wt.% $NaNO_3$ to apply to storage of energy; this mixture had a melting point of 140°C and a specific heat capacity of 1.56 kJ/kg K. Due to the very interesting characteristics of this ternary mixture, in the 1980s it was used as storage material in the experimental solar plant THEMIS, located in France. The main drawback of this salt mixture is that if it is heated above 350°C nitrites are produced from their oxidation with air;

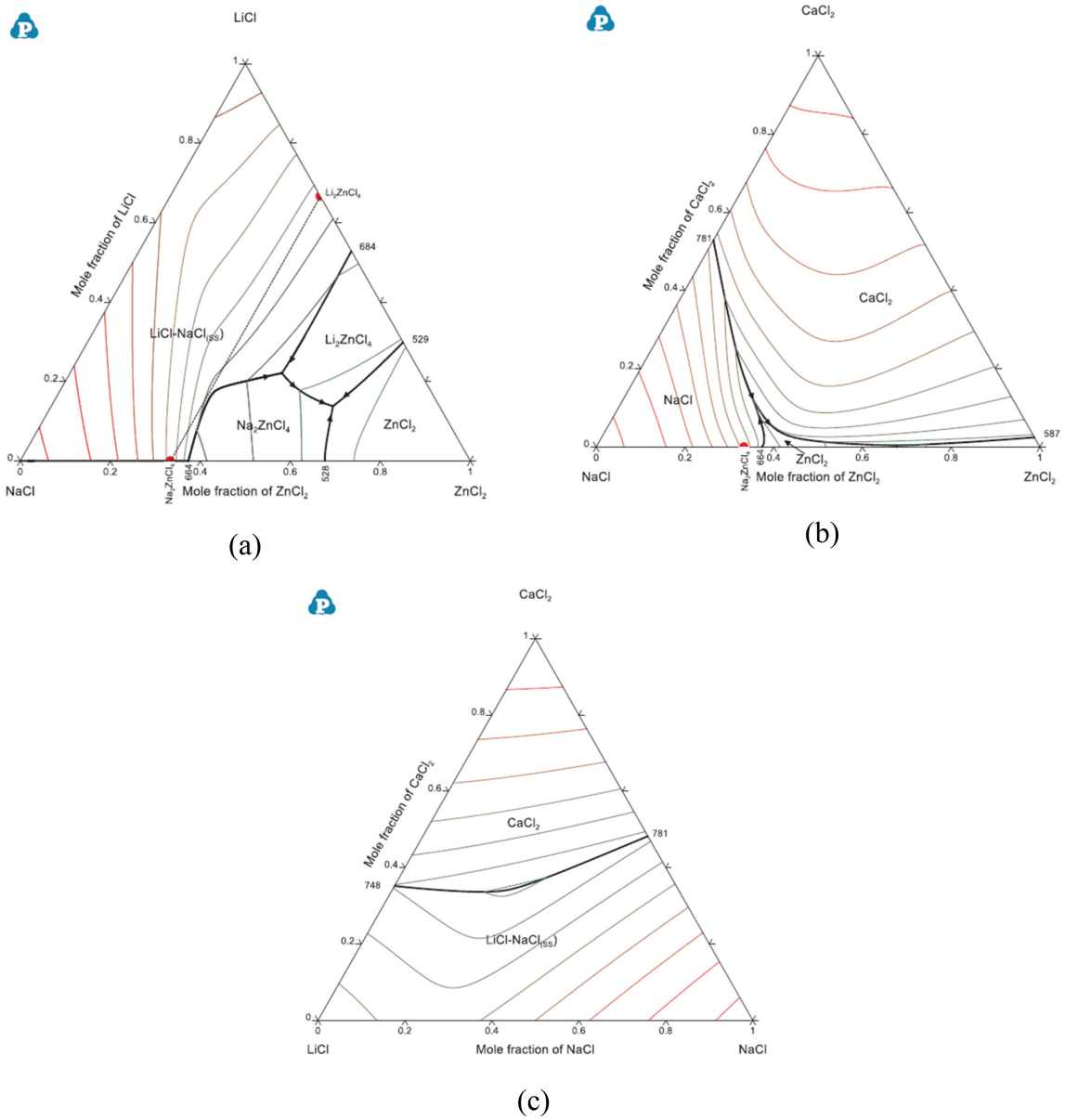


FIGURE 3 | Ternary diagrams developed by Wu et al. [14]. (a) LiCl–NaCl–$ZnCl_2$, (b) NaCl–$CaCl_2$–$ZnCl_2$, and (c) LiCl–NaCl–$CaCl_2$ phase diagram.

TABLE 3 | Proposed materials with nanoparticles used in sensible TES for CSP plants.

Material	Nanoparticles added	Heat capacity [kJ/kg K]	Stability limit [°C]	Reference
34 wt.% $BaCl_2$+13 wt.% NaCl+40 wt.% $CaCl_2$	1 wt.% SiO_2	0.98 ± 0.03 (14.5% enhancement)	n.a.	[17]

Abbreviation: n.a. – not available.

25784862, 2024, 8, Downloaded from https://onlinelibrary.wiley.com/doi/10.1002/est2.70091 by Makerere University, Wiley Online Library on [01/11/2026]. See the Terms and Conditions (https://onlinelibrary.wiley.com/terms-and-conditions) on Wiley Online Library for rules of use; OA articles are governed by the applicable Creative Commons License

therefore, also a gas cover with an inert gas is needed. These additional costs imply that the mixture is not used in commercial CSP plants.

Currently, the mixture used for TES in CSP plants is the so-called *Solar Salt*, a mixture of 60 wt.% $NaNO_3$+40 wt.% KNO_3. With this storage media, commercial CSP plants can reach up to 15 h of energy storage. The advantages of the mixtures are that the temperature range to use agrees with the high temperature and high pressure required in the steam turbines, they are in a liquid state at atmospheric pressure, their price is low according to their storage capacity, and they are neither flammable nor toxic.

The cost of the salts has become very important in commercial plants since the quantity used in TES systems is very large. An example is found in the new central receiver solar plant located in Chile, Cerro Dominador, which has 60 000 tons of *Solar Salt* for its TES system (designed for 17.5 h, 110 MW). Moreover, these commercial plants require that impurities content is below 0.02%. Therefore, development in the CSP sector is focused on reducing the cost of the storage media, the storage salts, in the different engineering designs developed worldwide and with proven operation. Optimizing physicochemical properties, such as heat capacity, melting point, or thermal stability, of salts increases the potential of improving them.

Cost reduction of a CSP plant is strongly influenced by the reduction of the required TES capacity, which can be achieved by increasing the maximum operating temperature, which leads to an increase in the thermal to electric conversion efficiency. New salt mixtures and salt chemistries are required to go to higher temperatures, since *Solar Salt* is limited to 565°C operating temperature, resulting in a net design point efficiency of 42%. Table 1 shows the candidates proposed in the literature to be used as TES materials at high temperatures, where NaCl can be found in several mixtures.

One of the proposed mixtures is composed of 20.4 wt.% KCl+55.1 wt.% $MgCl_2$+24.5 wt.% NaCl. The advantages of this mixture are its melting point (380°C), high thermal stability (it is stable until 800°C), and low vapor pressure. This mixture also overcomes some of the drawbacks of using $ZnCl_2$, including better heat capacity. However, disadvantages are also present in the use of this mixture, which is its highly corrosive nature. Corrosion mitigation approaches need to be assessed to achieve a corrosion rate in the container material lower than 20 μm/year, to ensure a plant lifetime of at least 30 years.

Literature shows that the main drivers of corrosion in molten chlorides are impurities such as H_2O, OH^-, O_2, and H^+. These impurities can break the passive surface oxide films formed in the container material that would protect it otherwise. In molten chlorides such as $MgCl_2$, one of the most important impurities is hydroxychlorides. These are formed when $MgCl_2$ is dried, via hydrolysis; hydroxychloride and HCl gas are formed at high temperatures with the reaction of chlorides with hydrated H_2O molecules. Thermal purification treatments can be used for corrosion resistance control since at higher temperatures, there is partial decomposition of hydroxychlorides forming HCl gas and its corresponding oxide.

Lately, chlorides have attracted attention from the CSP community as potential molten salts for storage. Such materials and mixtures are listed in Table 2.

The identification and optimization of suitable chloride salt mixtures for next-generation molten salt technology can be achieved through a thorough review of existing literature and/or through experimental measurements [15]. At first sight, alkali metal chloride salts such as KCl and NaCl, have better

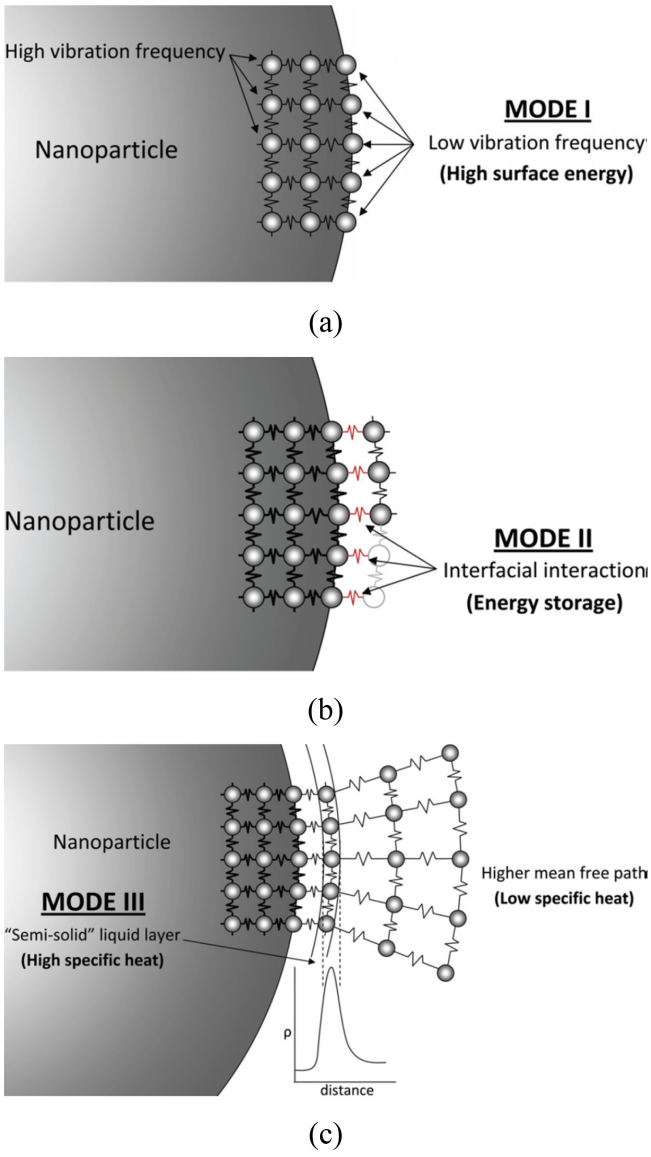


FIGURE 4 | Inclusion of nanoparticles in molten salts to enhance storage capacity modes: (a) Mode I: High surface energy of the surface atoms in the lattice. The low vibration frequency and higher amplitudes of vibration of these surface atoms contribute to increased energy storage capacity. (b) Mode II: Interfacial interactions between liquid molecules and lattice atoms, which are conceptualized as virtual spring-mass systems, to ease energy storage. (c) Mode III: Layer of semi-solid molecules adhering to the surface lattice atoms. This layer, characterized by reduced intermolecular spacing and semi-solid behavior, is expected to deliver a higher specific heat capacity. Notably, such a layer of semi-solid molecules would not form in the absence of nanoparticles. The mass density (ρ) is a key parameter in this context, measured in units of kg/m^3) [17].

25784862, 2024, 8, Downloaded from https://onlinelibrary.wiley.com/doi/10.1002/est2.70091 by Makerere University, Wiley Online Library on [01/11/2026]. See the Terms and Conditions (https://onlinelibrary.wiley.com/terms-and-conditions) on Wiley Online Library for rules of use; OA articles are governed by the applicable Creative Commons License

thermophysical properties than other chloride mixtures containing $CaCl_2$, and $MgCl_2$. Their advantages are higher heat capacity, lower vapor pressures at high temperatures, lower hygroscopicity, and lower costs; their main disadvantage is higher melting temperature (over 750°C). However, mixing these alkali metal chloride salts with alkaline earth metal chlorides (such as $MgCl_2$ or $CaCl_2$) can reduce their melting temperature. Among these considered salts, the binary mixture with the lowest temperature is KCl–$MgCl_2$, with a relatively low melting temperature of 426°C, low vapor pressure at high temperatures, and low cost. The addition of cheap NaCl can improve further such a mixture, decreasing even further its melting temperature, decreasing its cost, and increasing its heat capacity (Figure 1). The phase diagram of the ternary mixture consisting of $MgCl_2$, KCl, and NaCl was performed using the commercial software FactSage together with differential scanning calorimetry (DSC) measurements. The resulting diagram reveals the presence of a eutectic point with a composition of 55 wt.%/20.5 wt.%/24.5 wt.% that has a melting temperature of ~383°C.

It is interesting to know that some of these mixtures were first studied as heat transfer fluid and not for storage purposes, this is the case of 23.9 wt.% KCl+7.5 wt.% NaCl +68.6 wt.% $ZnCl_2$ [11, 16]. It should also be highlighted that a lot of corrosion studies have been developed related to chlorides to be used as molten salts, and moreover, how the impurities of the salts may influence their behavior and their potential interaction with gases to be used as a cover gas in the storage tanks [11]. The summary of the corrosion behavior can be found later in this paper.

Wu et al. [14] developed a thermodynamic description of the LiCl–NaCl–$CaCl_2$–$ZnCl_2$ system based on computational thermodynamic principles, showing that the ternary mixtures LiCl–NaCl–$ZnCl_2$ and NaCl–$CaCl_2$–$ZnCl_2$ had the potential to be used as thermal storage media. Figure 2 shows the phase diagram of the binary mixture NaCl–$ZnCl_2$. According to this study, the eutectic point and the peritectic point were located at 528 K and $x(ZnCl_2)=0.677$ and 664 K and $x(ZnCl_2)=0.374$, respectively. For the mixture NaCl–$CaCl_2$, the eutectic reaction liquid = α(NaCl)+$CaCl_2$ is located at 784 K and $x(CaCl_2)=0.528$.

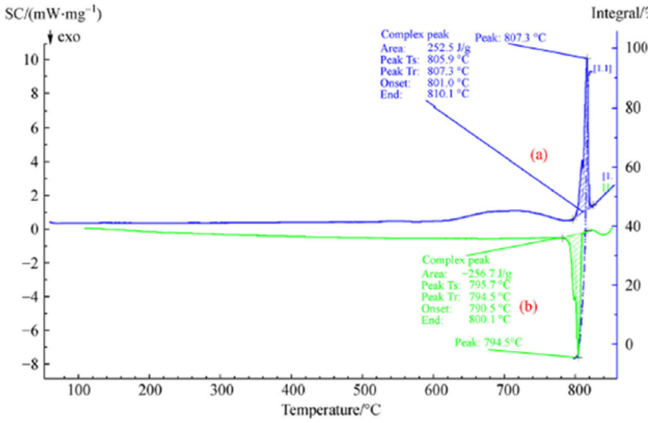
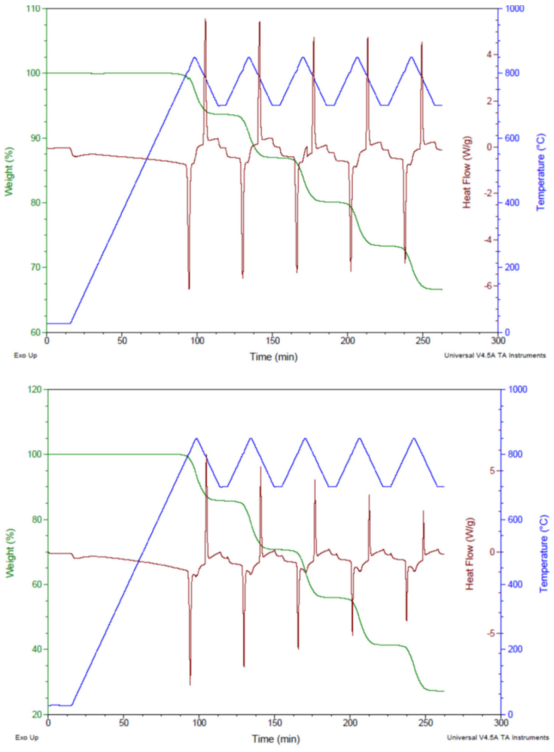


FIGURE 5 | (a) Melting and (b) Solidification segment curves of NaCl–Al2O_3 composite material fabricated at 140°C, 400 MPa with a holding time of 50 min [19].



(a)



(b)

FIGURE 6 | NaCl pellets with hemicellulose encapsulated with TiO_2 coating [7]. (a) Image; (b) TGA/DSC analysis (top, using dense TiO_2; bottom, using porous TiO_2).

25784862, 2024, 8, Downloaded from https://onlinelibrary.wiley.com/doi/10.1002/est2.70091 by Makerere University, Wiley Online Library on [01/11/2026]. See the Terms and Conditions (https://onlinelibrary.wiley.com/terms-and-conditions) on Wiley Online Library for rules of use; OA articles are governed by the applicable Creative Commons License

TABLE 4 | Some compositions used as PCM containing NaCl.

Material	Melting temperature [°C]	Melting enthalpy [J/g]	Stability limit [°C]	Reference
22.4 wt.% NaCl+77.6 wt.% H_2O	−21	228.14	n.a.	[21]
10 wt.% NaCl+90 wt.% H_2O	−8	289.9	n.a.	[22]
5 wt.% glycine+1 wt.% NaCl+94 wt.% H_2O	5	339.15	n.a.	[23]
3.1 wt.% LiCl+4.8 wt.% NaCl+27.1 wt.% KCl+65.0 wt.% $ZnCl_2$	170.8	69.8	500	[24]
87.36 wt.% $NaNO_3$+8.59 wt.% $LiNO_3$+4.05% NaCl	259.4	230.2	550	[25]
87.3 mol% NaOH+6.1 mol% NaCl+6.6 mol% Na_2CO_3	291	287	n.a.	[26]
80 wt.% NaOH+20 wt.% NaCl	370	370	n.a.	[27]
48 wt.% NaCl+52 wt.% $MgCl_2$	450	430	n.a.	[26]
50 mol% $CaCl_2$+7.25 mol% KCl+42.75 mol% NaCl	465	245	n.a.	[26]
33 wt.% NaCl+67 wt.% $CaCl_2$	500	393	n.a.	[26]
66 wt.% $CaCl_2$+5 wt.% KCl+29 wt.% NaCl	504	279	n.a.	[28]
53 wt.% $BaCl_2$+28 wt.% KCl+19 wt.% NaCl	542	165	640	[29]
25 wt.% NaCl+33 wt.% KCl+42 wt.% Na_2CO_3	569	249	n.a.	[30]
48 wt.% NaCl+52 wt.% Na_2CO_3	580	339	n.a.	[30]
68.05 wt.% Na_2SO_4+31.95 wt.% NaCl	625	263	700	[31]
59.45 wt.% Na_2CO_3+40.55 wt.% NaCl	635	312	700	[32, 33]
50 mol% KCl+50 mol% NaCl	656.85	312.8	n.a.	[34]
33.5 mol% NaF+6.5 mol% NaCl	675	572	800	[35]

Abbreviation: n.a. – not available.

Finally, for the binary mixture LiCl–NaCl, the calculated minimum was located at 819 K and x(NaCl) = 0.275, and solid–solid demixing was determined at 526 K and x(NaCl) = 0.330.

Figure 3 shows that the phase diagrams of the ternary mixtures LiCl–NaCl–$ZnCl_2$, NaCl–$CaCl_2$–$ZnCl_2$, and LiCl–NaCl–$CaCl_2$ could be predicted using the Kohler–Toop interpolation method and directly based on the optimized thermodynamic database of all the subsystems [14].

Table 3 lists chloride-based molten salt mixtures studied for the same application, where nanoparticles were added to improve their thermophysical properties [17, 18]. It is interesting to see that the authors claim that the addition of nanoparticles in the molten salts increases their storage capacity, although this is a very controversial issue within researchers. Shin and Barnerjee [17] discussed three potential independent competing inter-molecular interaction modes or mechanisms that could explain such enhancement of the specific heat capacity (Figure 4).

2.2 | NaCl as PCM

There are several studies where NaCl is used as PCM. For example, Suleiman et al. [19] developed a new composite with NaCl, by sintering it with Al_2O_3 (50–50 wt.%). Their innovative composite has a density that was 98.65% of that of the theoretical

25784862, 2024, 8, Downloaded from https://onlinelibrary.wiley.com/doi/10.1002/es2.70091 by Makerere University, Wiley Online Library on [01/11/2026]. See the Terms and Conditions (https://onlinelibrary.wiley.com/terms-and-conditions) on Wiley Online Library for rules of use; OA articles are governed by the applicable Creative Commons License

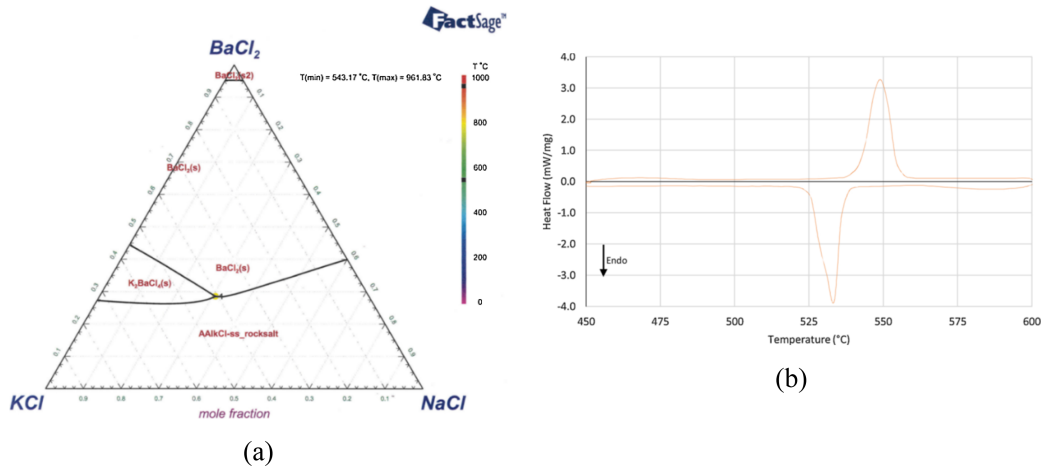


FIGURE 7 | (a) Phase Diagram of $BaCl_2$, KCl, NaCl [Factsage 6.4]; and (b) DSC curve of uncycled eutectic [29].

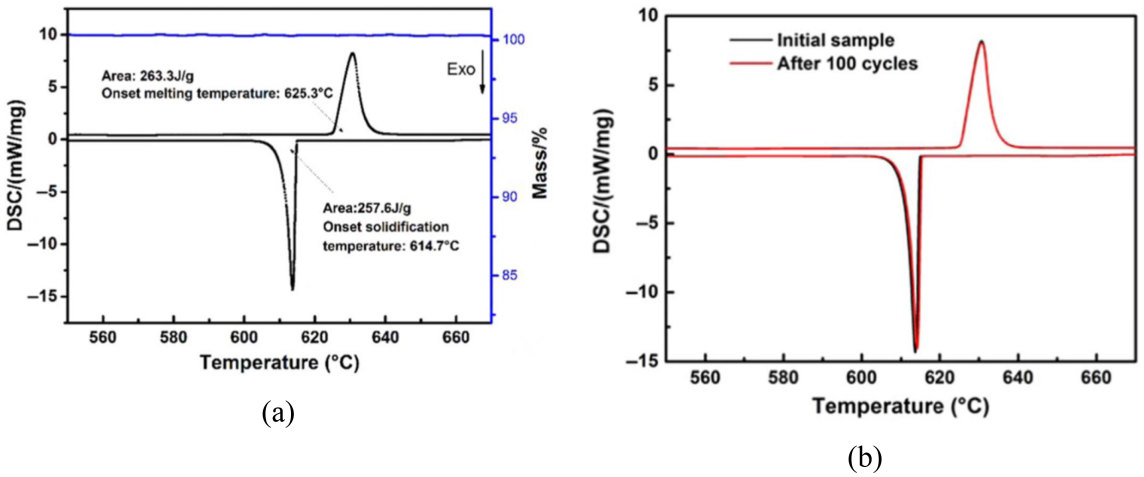


FIGURE 8 | (a) DSC–TG curves of eutectic Na_2SO_4–NaCl salt; (b) DSC curves of initial sample and 100-cycling of eutectic Na_2SO_4–NaCl [31].

one. Moreover, thermal cycling testing (30 cycles between 750°C and 850°C) showed that the NaCl–Al_2O_3 composite did not leak chloride salt. Simultaneous thermal analysis using a NETZSCH STA 449 F3 Jupiter apparatus gave a melting phase change of 252.5 J/g and a solidification phase change enthalpy of 256.7 J/g (Figure 5) [20].

Similarly, Arconada et al. [7] prepared a composite of NaCl pellets through the methodology sol–gel. The pelletization was carried out with six organic binders and then a PMMA coating was deposited as a sacrificial layer. The shell was produced by depositing titania (TiO_2) or silica (SiO_2) sol–gel coatings. Pellets fabricated with hemicellulose as a binder were fully characterized before and after five thermal cycles (Figure 6).

In the literature, different mixtures using NaCl identified as potential PCM can be found (Table 4).

In the search for PCMs for high-temperature applications, Jacob et al. [29] used FactSage to develop a new PCM with NaCl on its composition (with $BaCl_2$, KCl, and NaCl as components). Figure 6 shows a theoretical eutectic melting point of the ternary salt of 543.17°C and a latent heat of fusion to be 146 J/g. The final material tested was a mixture of 53 wt.% $BaCl_2$, 28 wt.% KCl, and 19 wt.% NaCl, with a melting temperature of 541.98°C and a melting enthalpy of 164.96 J/g.

Another potential PCM using NaCl was developed by Jiang et al. [31] with a final composition of 68.05 wt.% Na_2SO_4+31.95 wt.% NaCl, melting at 625.3°C with an enthalpy of 263.3 J/g. The mixture has good cycling reproducibility, but unfortunately has a subcooling of about 50°C (Figure 7).

Liu et al. [32, 33] developed the eutectic 59.45 wt.% Na_2CO_3+40.55 wt.% NaCl, a material with a melting temperature of 635°C and a melting enthalpy of 312 J/g, data comparable to previous literature. The eutectic showed good stability under thermal cycling and no subcooling (Figure 8a). This study also carried out corrosion tests of the new eutectic in contact with stainless steel. The corrosion rate increased linearly with the increasing number of cycles until 350 cycles. A stable passivation layer was formed around 350 cycles and further cycles up to 500 did not influence the corrosion rate (Figure 8b).

25784862, 2024, 8, Downloaded from https://onlinelibrary.wiley.com/doi/10.1002/est2.70091 by Makerere University, Wiley Online Library on [01/11/2026]. See the Terms and Conditions (https://onlinelibrary.wiley.com/terms-and-conditions) on Wiley Online Library for rules of use; OA articles are governed by the applicable Creative Commons License

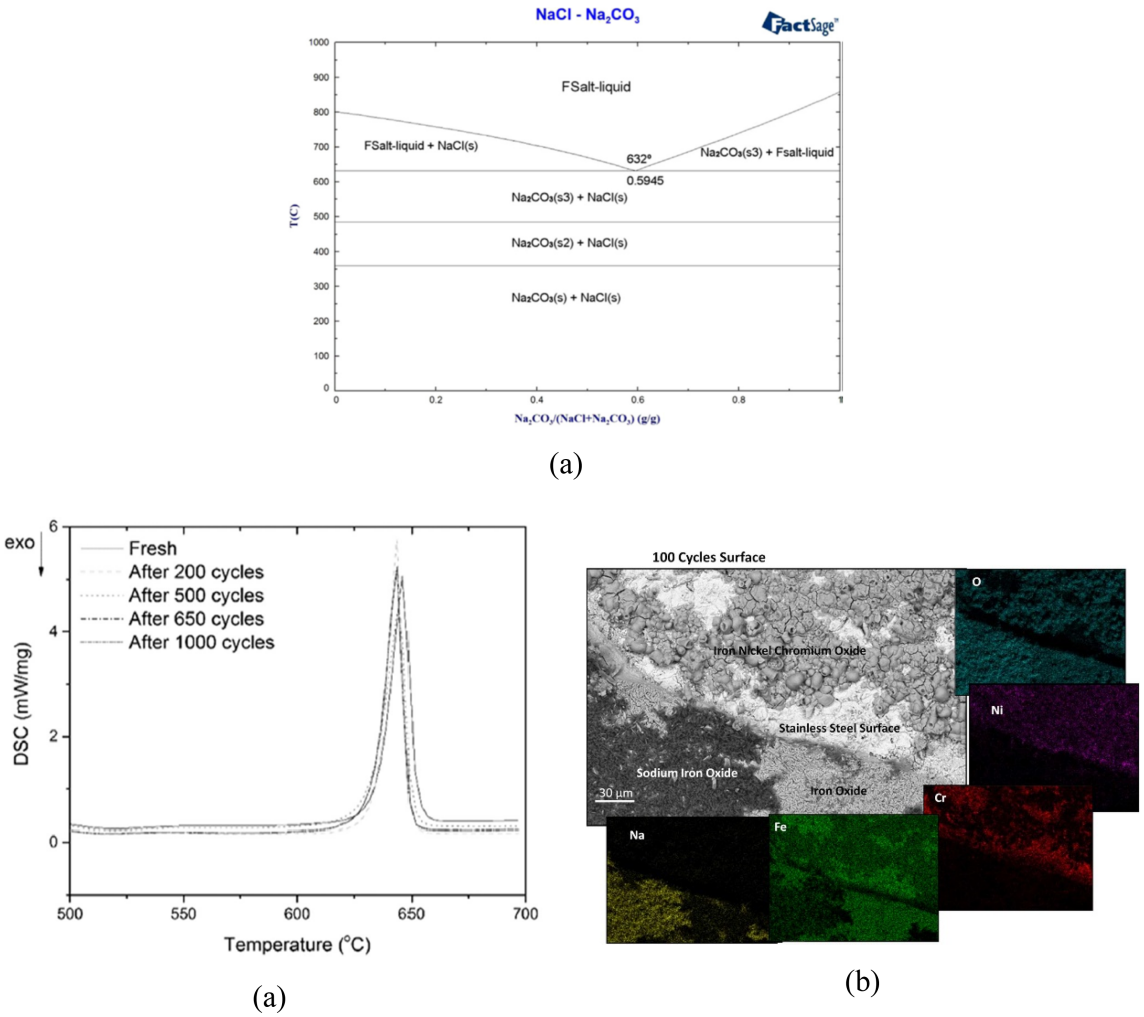


FIGURE 9 | (a) Phase diagram of NaCl–Na_2CO_3 salt generatedusingFactSage6.4, (b) DSC curves of eutectic NaCl–Na_2CO_3 after various numbers of thermal cycles, and (c) Example of corrosion results [32, 33].

Another interesting mixture containing NaCl and with the potential to be used as PCM is KCl–NaCl (50–50 mol%), with a melting point of 656.85°C and a melting enthalpy of 312.8 J/g [34] (Figure 9a,b). This mixture was analyzed previously by Mochinaga et al. [36], who developed its phase diagram finding that the eutectic is with the mixture 50.7–49.3 mol% (Figure 9c).

NaCl can also be mixed with fluorides to get new mixtures with potential to be used as PCM. Wang et al. [35] used an algorithm based on a back propagation artificial neural network (ANN) to develop a new mixture of NaCl and NaF; the algorithm was based on known salt data. Two new binary NaCl and NaF mixtures were predicted, and their composition and melting temperature were experimentally confirmed with an error lower than 1.5%. The melting temperature and melting enthalpy of the two eutectics were 648°C ± 2°C and 365 ± 5 J/g (Figure 10). Moreover, their thermal stability presented a weight loss lower than 3.0% up to 800°C.

It is interesting to see that some authors use NaCl as a way to modify the properties of the main PCM. For example, Li et al. [25] used sodium nitrate ($NaNO_3$) as the main PCM and added lithium nitrate ($LiNO_3$) and sodium chloride (NaCl) to prepare a ternary mixed molten salt. Authors claim that with this mixture, the melting point of the PCM decreases from 279.9°C to 259.4°C (Figure 11). Moreover, the authors claim that the melting enthalpy of the new mixture is higher than that of the individual salt, although they do not acknowledge that the melting curve of the mixture makes it very difficult to use in a real application. Finally, the TGA tests show that the new mixture starts its decomposition very soon after the melting, even though its degradation temperature is higher (550°C); on the other hand, cycling up to 30 cycles in the temperature range between 100°C and 350°C gave good results.

Authors used NaCl to develop new eutectic mixtures that could be used as PCM. For example, Lin et al. [24] developed the eutectic 3.1 wt.% LiCl+4.8 wt.% NaCl+27.1 wt.% KCl+65.0 wt.% $ZnCl_2$ and produced a composite with graphite with it. This material has a melting point of 170.8°C, but unfortunately, its freezing temperature is 121.1°C, therefore, it has a subcooling of 49.7°C, which undermines its possibility for commercial applications. Moreover, its low melting enthalpy (69.8 J/g) is also a drawback of this potential PCM (Figure 12).

A very different application of NaCl as PCM was presented by Padhye and Agrawal [22] and by Radebe et al. [21], who mixed NaCl with water as PCM for freezing applications. In

25784862, 2024, 8, Downloaded from https://onlinelibrary.wiley.com/doi/10.1002/es2.70091 by Makerere University, Wiley Online Library on [01/11/2026]. See the Terms and Conditions (https://onlinelibrary.wiley.com/terms-and-conditions) on Wiley Online Library for rules of use; OA articles are governed by the applicable Creative Commons License

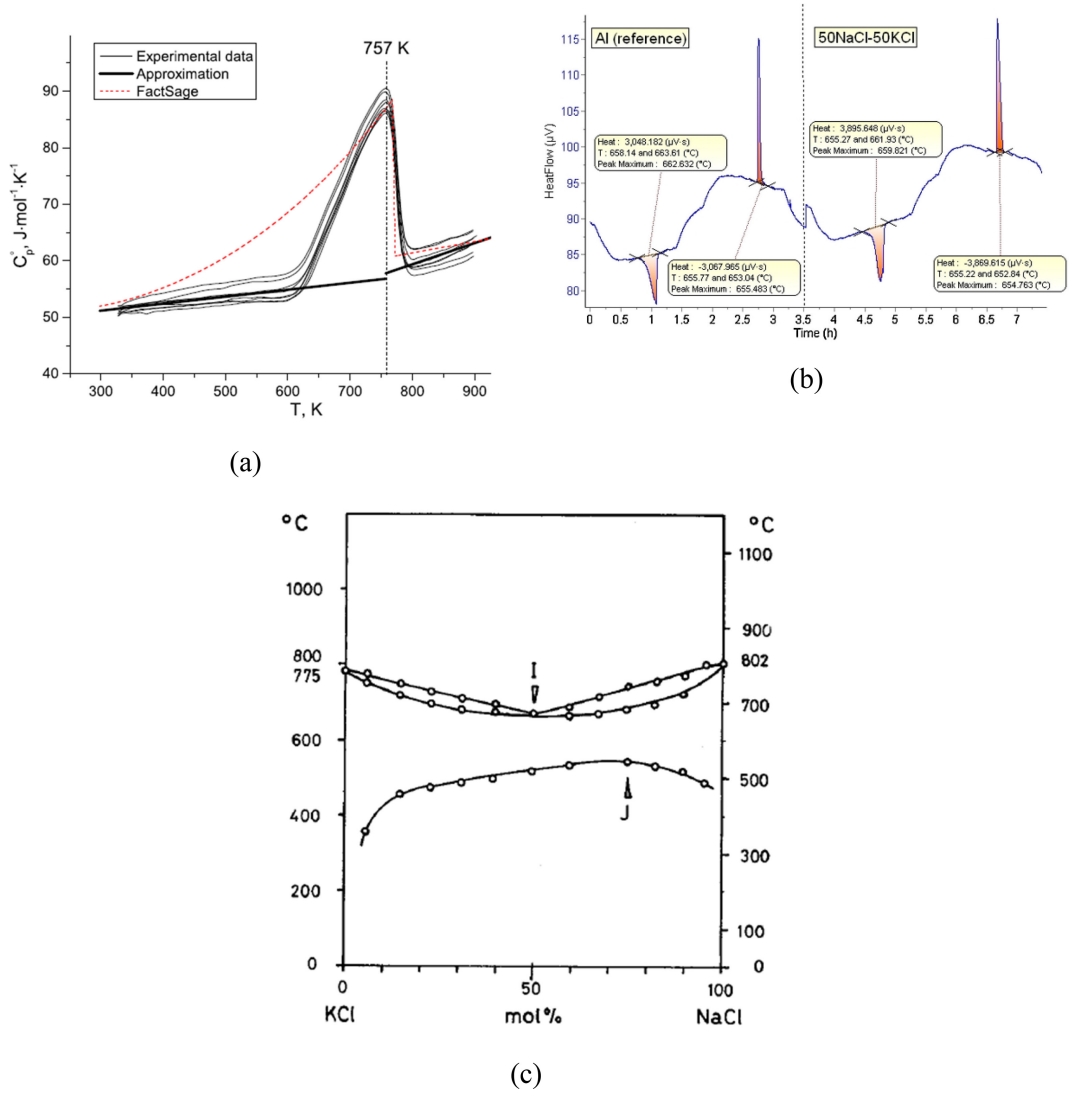


FIGURE 10 | (a) Heat capacity of the solid phase of 50 mol% NaCl–50% KCl, (b) calorimetry measurement [34], and (c) a phase diagram of the mixture NaCl–KCl [36].

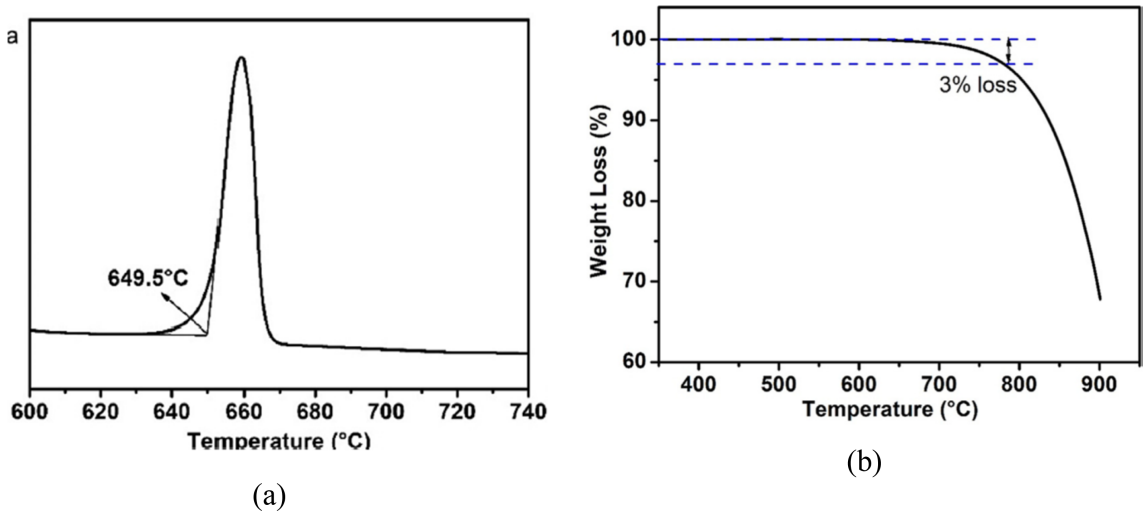


FIGURE 11 | DSC and TGS curves of reciprocal eutectic salt KCl–NaF [35]: (a) DSC, and (b) TGA.

25784862, 2024, 8, Downloaded from https://onlinelibrary.wiley.com/doi/10.1002/est2.70091 by Makerere University, Wiley Online Library on [01/11/2026]. See the Terms and Conditions (https://onlinelibrary.wiley.com/terms-and-conditions) on Wiley Online Library for rules of use; OA articles are governed by the applicable Creative Commons License

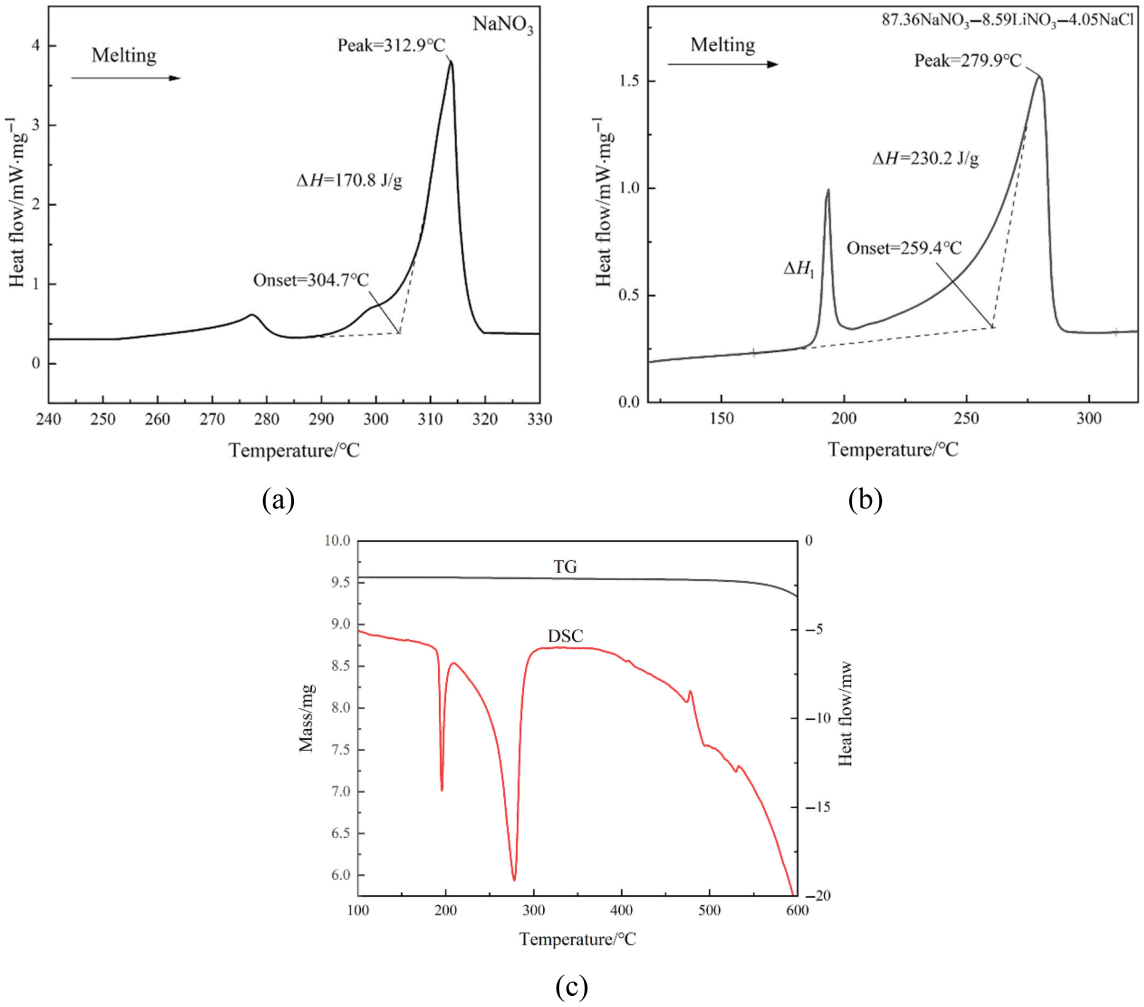


FIGURE 12 | Testing of sample: (a) DSC curve of $NaNO_3$ and (b) $NaNO_3$–$LiNO_3$–NaCl; and (c) TGA [25].

this case, NaCl is used as an additive to decrease the melting temperature of water while maintaining the interesting properties of water.

Similarly, Li et al. [23] used NaCl and glycine to develop new water-based PCMs for cold applications. The mixture 5 wt.% glycine +1 wt.% NaCl+94 wt.% H_2O has a melting temperature of 5°C and a melting enthalpy of 339.15 J/g, but also shows some subcooling.

3 | Corrosion Bibliographic Revision

The literature found that includes corrosion studies of chloride salts for TES is summarized in Table 5.

The corrosion rate is usually determined by calculating the mass loss on the metal piece immersed in the molten salt according to:

$$\mathrm{CR} = \frac{\Delta m}{\rho \cdot A} \cdot \frac{365 \cdot 24}{t} \cdot 10^4$$

where CR is the corrosion rate in μm/year; Δm is the difference in the mass of the metal after immersion test in g; ρ is the metal density in g/cm^3; A is the interfacial area between the metal and the molten salt in cm^2; and t refers to the time in hours.

Moreover, electrochemical techniques are also used for the evaluation of corrosion of metal samples in molten chlorides, mainly potentiodynamic polarization (PDP) and electrochemical impedance spectroscopy (EIS) [37, 38, 41–43]. In this case, the corrosion rate is calculated following the Faraday law [37, 38, 43]:

$$\mathrm{CR} = k \cdot \left[\frac{I_{\mathrm{corr}} \cdot \mathrm{EW}}{\rho \cdot A}\right]$$

where CR is the corrosion rate in μm/year; k is a constant with a value of 3.27 μm g/μA cm; meaning I_{corr} the corrosion current in μA; A represents the contact area between the working electrode (considered alloys) and molten chlorides; EW and ρ represent both the equivalent weight (dimensionless) and density in g/cm^3 of the metal sample, respectively [38].

Table 5 shows that both the temperature of the test and the atmosphere used (with oxygen or inert) have a significant effect on the corrosion rate of the metal samples. The corrosion rate

25784862, 2024, 8, Downloaded from https://onlinelibrary.wiley.com/doi/10.1002/est2.70091 by Makerere University, Wiley Online Library on [01/11/2026]. See the Terms and Conditions (https://onlinelibrary.wiley.com/terms-and-conditions) on Wiley Online Library for rules of use; OA articles are governed by the applicable Creative Commons License

TABLE 5 | Summary of corrosion studies of metal alloys in NaCl (adapted from [11]).

Molten salt	Alloy	T [°C]	Surrounding gases	Methodology	Rate of corrosion [μm/year]
24.0 wt.% KCl+7.4 wt.% NaCl+68.8 wt.% $ZnCl_2$	Hast N (~71 wt.% Ni)	250	Normal athosphere	Potentiodynamic polarization	37 [37]
		500	Normal athosphere	Potentiodynamic polarization	160 [37]
	Hast C-22 (~56 wt.% Ni)	250	Normal athosphere	Potentiodynamic polarization	16 [37] 14 [38]
		500	Normal athosphere	Potentiodynamic polarization	50 [37] 42 [38]
		400	Anaerobic conditions	Immersion test+mass loss (1000 h)	8 [38]
		800	Anaerobic conditions	Immersion test+mass loss (1000 h)	14 [38]
	Hast C-276 (~57 wt.% Ni)	250	Normal athosphere	Potentiodynamic polarization	11 [37]
		500	Normal athosphere	Potentiodynamic polarization	42 [37] 40 [38]
		500	Normal athosphere	Immersion test+mass loss (1000 h)	80 [38]
		800	Normal athosphere	Potentiodynamic polarization	500 [38]
		400	Anaerobic conditions	Immersion test+mass loss (1000 h)	3 [38]
		800	Anaerobic conditions	Immersion test+mass loss (1000 h)	4 [38]
	SS-304 (~8–11 wt.% Ni)	250	Normal athosphere	Potentiodynamic polarization	22 [37]
		500	Normal athosphere	Potentiodynamic polarization	381 [37]
		400	Anaerobic conditions	Immersion test+mass loss (1000 h)	14 [37]
43.6 wt.% $CaCl_2$+17.7 wt.% $MgCl_2$+38.7 wt.% NaCl	Inn-625 (~62 wt.% Ni)	600	Normal athosphere	Immersion test+mass loss (504 h)	121 [39]
	Hast X (~47 wt.% Ni)	600	Normal athosphere	Immersion test+mass loss (504 h)	153 [39]
	Hast B-3 (~65 wt.% Ni)	600	Normal athosphere	Immersion test+mass loss (504 h)	144 [39]
20.4 wt.% KCl+55.1 wt.% $MgCl_2$+24.5 wt.% NaCl	SS-304 (~8-11 wt.% Ni)	450–500	No-atmosphere	Immersion test+mass loss (1000 h)	< 10 [40]
		900	N_2-(0.1%–1%H_2O)-(1%–10%O_2)	Immersion test+mass loss (144 h)	Disintegrated [40]
	SS-316 (~10–14 wt.% Ni)	450–500	No-atmosphere	Immersion test+mass loss (1000 h)	~10 [40]
		900	N_2-(0.1%–1%H_2O)-(1%–10%O_2)	Immersion test+mass loss (144 h)	Disintegrated [40]
	SS-347 (~9–12 wt.% Ni)	450–500	No-atmosphere	Immersion test+mass loss (1000 h)	~120 [40]
	Hast N (~71 wt.% Ni)	450–500	No-atmosphere	Immersion test+mass loss (1000 h)	~50 [40]
	Inl-800H (~30–35 wt.% Ni)	900	N_2-(0.1%–1%H_2O)-(1%–10%O_2)	Immersion test+mass loss (144 h)	23 725 [40]
	Hast 230 (~57 wt.% Ni)	900	N_2-(0.1%–1%H_2O)-(1%–10%O_2)	Immersion test+mass loss (144 h)	20 345 [40]

(Continues)

25784862, 2024, 8, Downloaded from https://onlinelibrary.wiley.com/doi/10.1002/est2.70091 by Makerere University, Wiley Online Library on [01/11/2026]. See the Terms and Conditions (https://onlinelibrary.wiley.com/terms-and-conditions) on Wiley Online Library for rules of use; OA articles are governed by the applicable Creative Commons License

TABLE 5 | (Continued)

Molten salt	Alloy	T [°C]	Surrounding gases	Methodology	Rate of corrosion [μm/year]
53.3 wt.% KCl+41.7 wt.% NaCl+5.0 wt.% VCl_2	SS-316 L (~13.5–15 wt.% Ni)	750	Ar	Immersion test+mass loss (6 h)	54 000 [41]
		750	Ar	Potentiodynamic polarization (6 h)	1600 [41]
	SS-316Ti (~12–14 wt.% Ni)	750	Ar	Immersion test+mass loss (6 h)	61 000 [41]
		750	Ar	Potentiodynamic polarization (6 h)	7000 [41]
	SS-321 (~9–11 wt.% Ni)	750	Ar	I+M (6 h)	22 200 [41]
		750	Ar	Potentiodynamic polarization (6 h)	15 100 [41]
56.1 wt.% KCl+43.9 wt.% NaCl	SS-316 L (~13.5–15 wt.% Ni)	750	Ar	Immersion test+mass loss (80 h)	~157 [42]
	SS-316Ti (~12–14 wt.% Ni)	750	Ar	Immersion test+mass loss (80 h)	~168 [42]
	SS-321 (~9–11 wt.% Ni)	750	Ar	Immersion test+mass loss (80 h)	~225 [42]
55.8 wt.% KCl+44.2 wt.% LiCl	SS-304 (~8–11 wt.% Ni)	400	Anaerobic conditions	Immersion test+mass loss	2 [40]
		500	Anaerobic conditions	Immersion test+mass loss	6 [40]
	SS-316 (~10–14 wt.% Ni)	400	Anaerobic conditions	Immersion test+mass loss	2 [40]
	SS-347 (~9–12 wt.% Ni)	500	Anaerobic conditions	Immersion test+mass loss	2 [40]
68.6 wt.% LiCl+34.4 wt.% NaCl	SS 347 (~9–12 wt.% Ni)	650	N_2	Potentiodynamic polarization	7490 [43]
	SS 310 (~20.5 wt.% Ni)	650	N_2	Potentiodynamic polarization	6420 [43]
		700	N_2	Potentiodynamic polarization	12 450 [43]
	Inl 800H (30–35 wt.% Ni)	650	N_2	Potentiodynamic polarization	5940 [43]
		700	N_2	Potentiodynamic polarization	14 310 [43]
	Inn 625 (~62 wt.% Ni)	650	N_2	Potentiodynamic polarization	2800 [43]
52 wt.% $MgCl_2$+48 wt.% NaCl	Ni (> 99.97 wt.% Ni)	520	Normal athosphere	Immersion test+mass loss (140 h)	57 [44]
	GH-4033 (72.1 wt.% Ni+20.5 wt.% Cr+4.0 wt.% Fe+0.8 wt.% Al)	520	Normal athosphere	Immersion test+mass loss (140 h)	142 [44]
	GH-4169 (52.9 wt.% Ni+19.0 wt.% Cr+18.5 wt.% Fe+0.9 wt.% Ti+0.84 wt.% Al+3.1 wt.% Mo+5.2 wt.% Nb)	520	Normal athosphere	Immersion test+mass loss (140 h)	246 [44]

Abbreviations: Hast—Hastelloy; Inl—Incoloy (Ni wt.% < 50%); Inn—Inconel (Ni wt.% > 50%); SS—Stainless steel.

25784862, 2024, 8, Downloaded from https://onlinelibrary.wiley.com/doi/10.1002/esi2.70091 by Makerere University, Wiley Online Library on [01/11/2026]. See the Terms and Conditions (https://onlinelibrary.wiley.com/terms-and-conditions) on Wiley Online Library for rules of use; OA articles are governed by the applicable Creative Commons License

increases with increasing temperature, especially above 600°C [38]. Also oxidizing atmospheres (such as oxygen and water presence) increase the corrosion rate [38, 41, 43]. These data also show that nickel-based alloys (i.e., Incoloy, Inconel, Hastelloy) typically exhibit higher corrosion resistance in molten chloride environments as compared with stainless steel [43, 44]. Moreover, literature shows that impurities in the molten chlorides lead to higher corrosion rates [15].

Different corrosion mitigation methods have been investigated. For example, the addition of corrosion inhibitors [45–47] or the formation of a protective layer [48–50]. A known method to prevent metallic corrosion in aqueous solutions is cathodic protection by two methods, with a sacrificial anode or with an impressed current applied to the alloy. Another protection method that decreases corrosion on metals in contact with chlorides is the formation of a protective passivation layer. Coating can also be used, but to choose the right coating thermal stress, corrosion environment, or the potential dissolution of the protection layer within the molten salts should be considered [50].

4 | Conclusions

This study shows that NaCl has the potential to be used in TES for different applications, from low-temperature applications, such as food preservation and transport, to high-temperature applications, such as TES in CSP plants or in industry. NaCl has been proposed as a storage material using both sensible TES and latent TES, but there are no studies using NaCl for thermochemical TES. It is interesting to highlight that most studies evaluate mixtures of NaCl with other salts, and only a few consider NaCl by itself but producing compounds to be used as PCM.

Author Contributions

Conceptualization: L.F.C. Methodology: L.F.C. and G.Z. Investigation: E.B. and R.M. Resources: L.F.C. Data curation: L.F.C. Writing – original draft preparation: R.M. and L.F.C. Writing – review and editing: G.Z. and E.B. Supervision: L.F.C. Project administration: L.F.C. Funding acquisition: L.F.C. All authors have read and agreed to the published version of the manuscript.

Acknowledgments

This work was partially funded by the Ministerio de Ciencia e Innovación—Agencia Estatal de Investigación (AEI) (PID2021-123511OB-C31—MCIN/AEI/10.13039/501100011033/FEDER, UE), and Ministerio de Ciencia e Innovación—Agencia Estatal de Investigación (AEI) (RED2022-134219-T). Franklin R. Martinez Alcocer thanks the National Doctorate Scholarship for foreign students ANID 2021 Folio 21211932 for the financial support in the research. This work is partially supported by ICREA under the ICREA Academia program. The authors would like to thank the Catalan Government for the quality accreditation given to their research group (2021 SGR 01615). GREiA is a certified agent of TECNIO in the category of technology developers from the Government of Catalonia.

Conflicts of Interest

The authors declare no conflicts of interest.

Data Availability Statement

The data that support the findings of this study are available on request from the corresponding author. The data are not publicly available due to privacy or ethical restrictions.

References

1. L. F. Cabeza, "Introduction to the Section on Thermodynamics of Energy Storage," in *Encyclopedia of Energy Storage* (Netherlands: Elsevier, 2022), 1–4, https://doi.org/10.1016/B978-0-12-819723-3.00157-8.

2. L. F. Cabeza, I. Martorell, L. Miró, et al., "Introduction to Thermal Energy Storage Systems," in *Advances in Thermal Energy Storage Systems* (Elsevier, 2021), 1–33, https://doi.org/10.1016/B978-0-12-819885-8.00001-2.

3. L. F. Cabeza, E. Galindo, C. Prieto, C. Barreneche, and A. I. Fernández, "Key Performance Indicators in Thermal Energy Storage: Survey and Assessment," *Renewable Energy* 83 (2015): 820–827, https://doi.org/10.1016/j.renene.2015.05.019.

4. E. E. Michaelides, "Thermodynamics, Energy Dissipation, and Figures of Merit of Energy Storage Systems—A Critical Review," *Energies (Basel)* 14 (2021): 6121, https://doi.org/10.3390/en14196121.

5. J. Gasia, L. Miró, and L. F. Cabeza, "Review on System and Materials Requirements for High Temperature Thermal Energy Storage. Part 1: General Requirements," *Renewable and Sustainable Energy Reviews* 75 (2017): 1320–1338, https://doi.org/10.1016/j.rser.2016.11.119.

6. J. Gasia, L. Miró, and L. F. Cabeza, "Materials and System Requirements of High Temperature Thermal Energy Storage Systems: A Review. Part 2: Thermal Conductivity Enhancement Techniques," *Renewable and Sustainable Energy Reviews* 60 (2016): 1584–1601, https://doi.org/10.1016/j.rser.2016.03.019.

7. N. Arconada, L. Arribas, B. Lucio, J. González-Aguilar, and M. Romero, "Macroencapsulation of Sodium Chloride as Phase Change Materials for Thermal Energy Storage," *Solar Energy* 167 (2018): 1–9, https://doi.org/10.1016/j.solener.2018.02.045.

8. S. Ushak, A. G. Fernández, C. Prieto, and M. Grageda, "Advances in Molten Salt Storage Systems Using Other Liquid Sensible Storage Media for Heat Storage," in *Advances in Thermal Energy Storage Systems* (Elsevier, 2021), 55–81, https://doi.org/10.1016/B978-0-12-819885-8.00003-6.

9. G. Picard, "Process for Stabilizing a Mixture of Molten Alkali Metal Nitrates and Alkali Metal Nitrites Usable Particularly as a Heat Transfer Fluid and Stabilized Mixture Thus Obtained," 1985, US4559993.

10. H. Mehling and L. F. Cabeza, *Heat and Cold Storage With PCM. An up to Date Introduction Into Basics and Applications*, 1st ed. (Berlin Heidelberg, Berlin, Germany: Springer-Verlag, 2008), https://doi.org/10.1007/978-3-540-68557-9.

11. W. Ding, A. Bonk, and T. Bauer, "Corrosion Behavior of Metallic Alloys in Molten Chloride Salts for Thermal Energy Storage in Concentrated Solar Power Plants: A Review," *Frontiers of Chemical Science and Engineering* 12 (2018): 564–576, https://doi.org/10.1007/s11705-018-1720-0.

12. A. M. Kruizenga, "Corrosion Mechanisms in Chloride and Carbonate Salts. SANDIA Report SAND2012-7594," 2012.

13. M. Mehos, C. Turchi, J. Vidal, et al., "Concentrating Solar Power Gen3 Demonstration Roadmap," 2017.

14. S. Wu, H. Peng, and L. Xie, "Design and Investigation of the Novel $ZnCl_2$ Based Ternary Chloride Salts With Low-Temperature for Sensible Energy Storage," *Applied Thermal Engineering* 171 (2020): 114917, https://doi.org/10.1016/j.applthermaleng.2020.114917.

15. W. Ding and T. Bauer, "Progress in Research and Development of Molten Chloride Salt Technology for Next Generation Concentrated

25784862, 2024, 8, Downloaded from https://onlinelibrary.wiley.com/doi/10.1002/est2.70091 by Makerere University, Wiley Online Library on [01/11/2026]. See the Terms and Conditions (https://onlinelibrary.wiley.com/terms-and-conditions) on Wiley Online Library for rules of use; OA articles are governed by the applicable Creative Commons License

Solar Power Plants," *Engineering* 7 (2021): 334–347, https://doi.org/10.1016/j.eng.2020.06.027.

16. K. Vignarooban, X. Xu, A. Arvay, K. Hsu, and A. M. Kannan, "Heat Transfer Fluids for Concentrating Solar Power Systems—A Review," *Applied Energy* 146 (2015): 383–396, https://doi.org/10.1016/j.apenergy.2015.01.125.

17. D. Shin and D. Banerjee, "Enhancement of Specific Heat Capacity of High-Temperature Silica-Nanofluids Synthesized in Alkali Chloride Salt Eutectics for Solar Thermal-Energy Storage Applications," *International Journal of Heat and Mass Transfer* 54 (2011): 1064–1070, https://doi.org/10.1016/j.ijheatmasstransfer.2010.11.017.

18. A. G. Fernández, J. Gomez-Vidal, E. Oró, A. Kruizenga, A. Solé, and L. F. Cabeza, "Mainstreaming Commercial CSP Systems: A Technology Review," *Renewable Energy* 140 (2019): 152–176, https://doi.org/10.1016/j.renene.2019.03.049.

19. B. Suleiman, Q. Yu, Y. Ding, and Y. Li, "Fabrication of Form Stable NaCl-Al_2O_3 Composite for Thermal Energy Storage by Cold Sintering Process," *Frontiers of Chemical Science and Engineering* 13 (2019): 727–735, https://doi.org/10.1007/s11705-019-1823-2.

20. J. Zhu, R. Li, W. Zhou, H. Zhang, and X. Cheng, "Fabrication of Al_2O_3-NaCl Composite Heat Storage Materials by One-Step Synthesis Method," *Journal of Wuhan University of Technology-Materials Science Edition* 31 (2016): 950–954, https://doi.org/10.1007/s11595-016-1473-x.

21. T. B. Radebe, A. U. C. Ndanduleni, and Z. Huan, "Investigation of Low-Cost Eutectic Salts to Ensure Food Products During Power Outages," *Journal of Energy Storage* 63 (2023): 106960, https://doi.org/10.1016/j.est.2023.106960.

22. M. S. Padhye and N. Agrawal, "Integration of Phase Change Materials (PCMs) in Freezer of a Domestic Refrigerator: A Comparative Study," *Journal of The Institution of Engineers (India): Series C* 104 (2023): 1057–1064, https://doi.org/10.1007/s40032-023-00972-7.

23. G. Li, Q. Yu, Y. Liu, M. Li, Y. Zhang, and Y. Wang, "The Efficient and Developing Phase Transition Freezing Materials Generated From Amino Acids," *Journal of Molecular Liquids* 382 (2023): 121933, https://doi.org/10.1016/j.molliq.2023.121933.

24. Z. Lin, Z. Zhao, J. Song, et al., "Chloride Salts/Graphite Foam Composites Prepared by Vacuum Impregnation With High Thermal Conductivity for Medium Temperature Thermal Energy Storage," *Thermal Science and Engineering Progress* 44 (2023): 102026, https://doi.org/10.1016/j.tsep.2023.102026.

25. Y. Li, S. H. Zhou, S. Wang, K. Q. Ma, and Q. Z. Zhu, "Preparation and Thermal Properties of a Novel Ternary Molten Salt/Expanded Graphite Thermal Storage Material," *Journal of Energy Storage* 74 (2023): 109273, https://doi.org/10.1016/j.est.2023.109273.

26. M. M. Kenisarin, "High-Temperature Phase Change Materials for Thermal Energy Storage," *Renewable and Sustainable Energy Reviews* 14 (2010): 955–970, https://doi.org/10.1016/j.rser.2009.11.011.

27. M. Liu, W. Saman, and F. Bruno, "Review on Storage Materials and Thermal Performance Enhancement Techniques for High Temperature Phase Change Thermal Storage Systems," *Renewable and Sustainable Energy Reviews* 16 (2012): 2118–2132, https://doi.org/10.1016/j.rser.2012.01.020.

28. G. Alva, L. Liu, X. Huang, and G. Fang, "Thermal Energy Storage Materials and Systems for Solar Energy Applications," *Renewable and Sustainable Energy Reviews* 68 (2017): 693–706, https://doi.org/10.1016/j.rser.2016.10.021.

29. R. Jacob, M. Liu, Y. Sun, M. Belusko, and F. Bruno, "Characterisation of Promising Phase Change Materials for High Temperature Thermal Energy Storage," *Journal of Energy Storage* 24 (2019): 100801, https://doi.org/10.1016/j.est.2019.100801.

30. S. Riahi, M. Liu, R. Jacob, M. Belusko, and F. Bruno, "Assessment of Exergy Delivery of Thermal Energy Storage Systems for CSP Plants: Cascade PCMs, Graphite-PCMs and Two-Tank Sensible Heat Storage Systems," *Sustainable Energy Technologies and Assessments* 42 (2020): 100823, https://doi.org/10.1016/j.seta.2020.100823.

31. Y. Jiang, Y. Sun, R. D. Jacob, F. Bruno, and S. Li, "Novel Na2SO4-NaCl-Ceramic Composites as High Temperature Phase Change Materials for Solar Thermal Power Plants (Part I)," *Solar Energy Materials and Solar Cells* 178 (2018): 74–83, https://doi.org/10.1016/j.solmat.2017.12.034.

32. M. Liu, S. Bell, M. Segarra, et al., "A Eutectic Salt High Temperature Phase Change Material: Thermal Stability and Corrosion of SS316 With Respect to Thermal Cycling," *Solar Energy Materials and Solar Cells* 170 (2017): 1–7, https://doi.org/10.1016/j.solmat.2017.05.047.

33. Y. Jiang, Y. Sun, M. Liu, F. Bruno, and S. Li, "Eutectic Na2CO3–NaCl Salt: A New Phase Change Material for High Temperature Thermal Storage," *Solar Energy Materials and Solar Cells* 152 (2016): 155–160, https://doi.org/10.1016/j.solmat.2016.04.002.

34. D. Sergeev, D. Kobertz, and M. Müller, "Thermodynamics of the NaCl–KCl System," *Thermochimica Acta* 606 (2015): 25–33, https://doi.org/10.1016/j.tca.2015.03.003.

35. Y. Wang, C. Ling, H. Yin, W. Liu, Z. Tang, and Z. Li, "Thermophysical Properties of KCl-NaF Reciprocal Eutectic by Artificial Neural Network Prediction and Experimental Measurements," *Solar Energy* 204 (2020): 667–672, https://doi.org/10.1016/j.solener.2020.05.029.

36. J. Mochinaga, H. Ohtani, and K. Igarashi, "Phase Diagram of Ternary DyCl3-KCl-NaCl System," *Denki Kagaku oyobi Kogyo Butsuri Kagaku* 49 (1981): 19–21, https://doi.org/10.5796/kogyobutsurikagaku.49.19.

37. K. Vignarooban, P. Pugazhendhi, C. Tucker, D. Gervasio, and A. M. Kannan, "Corrosion Resistance of Hastelloys in Molten Metal-Chloride Heat-Transfer Fluids for Concentrating Solar Power Applications," *Solar Energy* 103 (2014): 62–69, https://doi.org/10.1016/j.solener.2014.02.002.

38. K. Vignarooban, X. Xu, K. Wang, et al., "Vapor Pressure and Corrosivity of Ternary Metal-Chloride Molten-Salt Based Heat Transfer Fluids for Use in Concentrating Solar Power Systems," *Applied Energy* 159 (2015): 206–213, https://doi.org/10.1016/j.apenergy.2015.08.131.

39. B. Liu, X. Wei, W. Wang, J. Lu, and J. Ding, "Corrosion Behavior of Ni-Based Alloys in Molten NaCl-$CaCl_2$-$MgCl_2$ Eutectic Salt for Concentrating Solar Power," *Solar Energy Materials and Solar Cells* 170 (2017): 77–86, https://doi.org/10.1016/j.solmat.2017.05.050.

40. G. Y. Lai, *High-Temperature Corrosion and Materials Applications* (United States: ASM International, 2007).

41. A. V. Abramov, I. B. Polovov, V. A. Volkovich, O. I. Rebrin, E. I. Denisov, and T. R. Griffiths, "Corrosion of Austenitic Steels and Their Components in Vanadium-Containing Chloride Melts," *ECS Transactions* 50 (2013): 685–698, https://doi.org/10.1149/05011.0685ecst.

42. A. V. Abramov, I. B. Polovov, V. A. Volkovich, and O. I. Rebrin, "Corrosion of Austenitic Stainless Steels in Chloride Melts," in *Molten Salts Chemistry and Technology*, eds. M. Gaune-Escard and G. M. Haarberg (Germany: Wiley, 2014), 427–448.

43. J. C. Gomez-Vidal and R. Tirawat, "Corrosion of Alloys in a Chloride Molten Salt (NaCl-LiCl) for Solar Thermal Technologies," *Solar Energy Materials and Solar Cells* 157 (2016): 234–244, https://doi.org/10.1016/j.solmat.2016.05.052.

44. J. Wang, C. Zhang, Z. Li, H. Zhou, J. He, and J. Yu, "Corrosion Behavior of Nickel-Based Superalloys in Thermal Storage Medium of Molten Eutectic NaCl-MgCl2 in Atmosphere," *Solar Energy Materials and Solar Cells* 164 (2017): 146–155, https://doi.org/10.1016/j.solmat.2017.02.020.

45. J. E. Indacochea, J. L. Smith, K. R. Litko, E. J. Karell, and A. G. Rarez, "High-Temperature Oxidation and Corrosion of Structural Materials in

25784862, 2024, 8, Downloaded from https://onlinelibrary.wiley.com/doi/10.1002/est2.70091 by Makerere University, Wiley Online Library on [01/11/2026]. See the Terms and Conditions (https://onlinelibrary.wiley.com/terms-and-conditions) on Wiley Online Library for rules of use; OA articles are governed by the applicable Creative Commons License

Molten Chlorides," *Oxidation of Metals* 55 (2001): 1–16, https://doi.org/10.1023/A:1010333407304.

46. J. E. Indacochea, J. L. Smith, K. R. Litko, and E. J. Karell, "Corrosion Performance of Ferrous and Refractory Metals in Molten Salts Under Reducing Conditions," *Journal of Materials Research* 14 (1999): 1990–1995, https://doi.org/10.1557/JMR.1999.0268.

47. B. L. Garcia-Diaz, L. Olson, M. Martinez-Rodriguez, R. Fuentes, H. Colon-Mercado, and J. Gray, "High Temperature Electrochemical Engineering and Clean Energy Systems," *Journal of the South Carolina Academy of Science* 14 (2016): 11–14.

48. J. C. Gomez-Vidal, A. G. Fernandez, R. Tirawat, C. Turchi, and W. Huddleston, "Corrosion Resistance of Alumina-Forming Alloys Against Molten Chlorides for Energy Production. I: Pre-Oxidation Treatment and Isothermal Corrosion Tests," *Solar Energy Materials and Solar Cells* 166 (2017): 222–233, https://doi.org/10.1016/j.solmat.2017.02.019.

49. J. C. Gomez-Vidal, "Corrosion Resistance of MCrAlX Coatings in a Molten Chloride for Thermal Storage in Concentrating Solar Power Applications," *npj Materials Degradation* 1 (2017): 7, https://doi.org/10.1038/s41529-017-0012-3.

50. K. Azarbayjani, G. Rizvi, and F. Foroutan, "Evaluating Effects of Immersion Tests in Molten Copper Chloride Salts on Corrosion Resistant Coatings," *International Journal of Hydrogen Energy* 41 (2016): 8394–8400, https://doi.org/10.1016/j.ijhydene.2015.10.092.

25784862, 2024, 8, Downloaded from https://onlinelibrary.wiley.com/doi/10.1002/est2.70091 by Makerere University, Wiley Online Library on [01/11/2026]. See the Terms and Conditions (https://onlinelibrary.wiley.com/terms-and-conditions) on Wiley Online Library for rules of use; OA articles are governed by the applicable Creative Commons License